NMR spin relaxation theory of biomolecules undergoing highly asymmetric exchange with large interaction partners

Gregory Jameson[†,‡] and Rafael Brüschweiler[*,†,‡,¶,§]

†*Department of Chemistry and Biochemistry, The Ohio State University, Columbus, Ohio 43210, United States*

‡*Biophysics Graduate Program, The Ohio State University, Columbus, Ohio 43210, United States*

¶*Department of Biological Chemistry and Pharmacology, The Ohio State University, Columbus, Ohio 43210, United States*

§*Current address: 151 W. Woodward Ave, The Ohio State University, Columbus, Ohio 43210*

E-mail: bruschweiler.1@osu.edu

Abstract

The transient interactions of proteins and other molecules with much larger structures, such as synthetic or biological nanoparticles, lead to certain types of enhanced nuclear magnetic resonance (NMR) spin relaxation effects, which can be accurately measured by multidimensional solution NMR techniques. These relaxation effects provide new information about the nanostructures and the protein, their interactions, internal dynamics and associated kinetic and thermodynamic parameters, such as exchange rates and populations. Although theoretical treatments exist that cover either the fast or slow exchange limits, a theoretical treatment that applies to all practically relevant exchange processes is still missing. A unified theoretical framework is presented for this purpose based on a stochastic Liouville equation (SLE). It covers nuclear spin dynamics, overall rotational diffusion of both the protein and the nanostructure, the exchange process between a free and a bound state, and internal protein dynamics. Although the numerical implementation of the SLE typically involves large matrices, it is shown here that it is computationally still tractable for situations relevant in practice. Application of the theory demonstrates how transverse relaxation is substantially impacted by the kinetics of binding on a wide range of exchange timescales. It is further shown that when exchange occurs on the appropriate timescale, transverse relaxation is able to report on internal dynamics far slower than observable by traditional transverse relaxation experiments. The SLE will allow the realistic and quantitative interpretation of experimental NMR data reporting about transient protein-nanoparticle interactions, thereby providing a powerful tool for the characterization of protein dynamics modes on a vast range of timescales including motions that may be functionally relevant.

INTRODUCTION

In living organisms, biological molecules including biomacromolecules, such as proteins or nucleic acids, interact with the complex chemical environment inside and outside of cells. These nanostructures can be much larger than the biological molecule itself, i.e. in the tens of nanometer range or beyond, for example in the form of a cell membrane, a ribosome, or an organelle, and hence they can undergo much slower rotational diffusion in solution or even have a static orientation. The situation is fully analogous if the nanostructure is synthetic in nature, such as an inorganic nanoparticle. Molecule-nanostructure interactions can be permanent or transient with sizeable kinetic on and off exchange rates. In either case, such interactions can be biologically important. However, the experimental characterization of transient interactions is challenging due to the often elusive nature of the bound state.

From a solution nuclear magnetic resonance (NMR) spectroscopic perspective, a molecule with long-lived interactions with large particles will have a very large spectral linewidth accompanied by low sensitivity impeding the direct observation of such complexes. However, in case that these interactions are transient, experiencing sufficiently rapid exchange, and have bound populations of the order of a few percent or even smaller, the resulting protein NMR spectra will still have a solution-NMR like appearance with high spectral resolution and good sensitivity. At the same time, these spectra encode unique information about properties of the nanostructure, the exchange process, and the protein molecule itself. In the following, we will refer to the observed species simply as "molecule" or "protein" (P) and the larger nanostructure with which it interacts as "nanoparticle" (NP).

NMR has a long history in harnessing information about molecules and their properties when undergoing exchange between a free state and a bound state. Such NMR techniques include the transferred NOE,[1–3] enhanced water relaxation through exchange,[4,5] saturation transfer difference (STD) NMR,[6,7] chemical exchange saturation transfer (CEST),[8,9] paramagnetic relaxation enhancement,[10,11] or dark state exchange saturation transfer (DEST).[12,13] We recently introduced nanoparticle-assisted spin relaxation (NASR) of proteins, which al-

lows one to characterize the internal protein dynamics on a much wider range of timescales than previously possible by standard NMR spin relaxation methods.[14,15] At the example of a ^{15}N spin, by measuring the difference between transverse spin relaxation rates $\Delta R_2(^{15}N) = R_{2,ex}(^{15}N) – R_{2,P}(^{15}N)$ in exchange with and absence of nanoparticles, a generalized S^2 order parameter could be be extracted for each protein resonance that reports on internal protein dynamics. The S^2 value obtained in this way is similar to that from a standard-model free analysis,[16] except that it reports on a much larger range of internal timescales from ps to μs, depending on the size of the nanoparticle. By contrast, model-free analysis applied to a set of standard NMR spin relaxation experiments measured in the absence of nanoparticles reports about internal dynamics on timescales from ps to low ns only, because internal motions on timescales that are of the order of or slower than the protein rotational diffusion correlation time, τ_P, become undetectable.

A thorough theoretical description of the effect of exchange phenomena on transverse relaxation, such as NASR, requires the proper mathematical treatment of such dynamics processes from both a spin dynamics and a lattice dynamics point of view. The Bloch-McConnell (BM) equation[17] is the most commonly used approach to describe the magnetic resonance properties of a molecule that is undergoing exchange between two states, bound vs. free, that have the same chemical shift but different R_2 relaxation times due to differences in the rotational diffusion correlation times (for reviews of BM, see[13,18]). The BM approach relies on the assumption that exchange is slow enough that it does not affect the R_2 relaxation times of each of the two states themselves, only their averaging properties, allowing one to treat the problem as kinetic exchange between two (or more) Bloch matrices. Moreover, the relaxation processes giving rise to R_1 and R_2 of the individual states are assumed to fall into the Redfield regime, i.e. their correlation times are much faster than the relaxation-active interactions or the relaxation times $1/R_2$, $1/R_1$, although the physical nature of the relaxation mechanism (dipolar, CSA, quadrupolar, etc.) is usually not specified. An alternative approach was introduced by Wong, Case, and Szabo (WCS),[19] where

an analytical time-correlation function was derived that describes a molecule undergoing the aforementioned exchange between two states. In contrast to BM, the WCS approach assumes that exchange occurs entirely within Redfield relaxation theory, and as such can be captured within the Bloch-Wangsness-Redfield time-correlation function framework. The dependence of ΔR_2 on k_{ex} of the BM and WCS approach is depicted Figure 1 (dashed lines). It shows the complementarity of BM and WCS covering either the exchange regime in the slow (BM) or fast exchange limit (WCS). However, neither approach is accurate in the intermediate k_{ex} regime and in the limits of slow and fast exchange the two approaches give divergent results.

Here, we introduce a unified theoretical treatment that is capable of accurately handling all exchange timescales and all overall tumbling correlation times. It is based on the solution of a stochastic Liouville equation (SLE).[20] SLE in different forms have previously found a number of useful applications in magnetic resonance.[21–31] Here, we present a SLE that simultaneously couples differential equations describing the following processes in spin and real space: (i) spin dynamics described by the Liouville-von Neumann equation,[32] (ii) two tumbling spherical tops described by their rotational diffusion differential equations,[1,33] (iii) the stochastic chemical exchange between the free and bound states, and (iv) internal dynamics by intramolecular multi-site exchange.[34–36] Although computationally more expensive than both BM and WCS treatments, the absence of certain important assumptions in the SLE treatment makes this approach more general than previous treatments thereby covering the more restricted applicability ranges of BM and WCS.

The type of predictions over a large parameter range made possible by the SLE is illustrated in Figure 1. It shows $\Delta R_2(^{15}N)$ for a small protein ($\sim$9 kDa, tumbling correlation time $\tau_P \cong 4ns$) in free solution in exchange with a nanoparticle-bound state, at 1% bound population, as a function of the exchange rate constant $k_{ex} = k_{on} + k_{off}$ as predicted by BM, WCS, and SLE treatments. As can be seen, SLE accurately reproduces the analytical relaxation behavior obtained from BM for exchange rates k_{ex} below roughly 10^4 s^{-1} and it also coincides with the relaxation properties obtained from WCS for exchange times above

$10^5\ s^{-1}$, thereby bridging the application regimes of the two approximate treatments. The figure shows how in the intermediate exchange regime between $10^4\ s^{-1}$ and $10^5\ s^{-1}$, both approximate treatments significantly deviate from the exact SLE results.

In the following sections, the SLE will be introduced in mathematical detail before it is applied to various scenarios to provide an understanding of the spin relaxation effects for different regimes of model parameters that describe the protein, its internal dynamics, and its exchange between a free state and a bound state on the surface of a slowly tumbling nanoparticle.

THEORY

The time evolution of a spin ensemble can be described by the Stochastic Liouville Equation (SLE) given by

$$\partial_t \hat{\rho}(\Omega, t) = -i\hat{\hat{L}}(\Omega)\hat{\rho}(\Omega, t) + \hat{\Gamma}\hat{\rho}(\Omega, t) \tag{1}$$

where $\hat{\rho}(\Omega, t)$ is the deviation of the ensemble-averaged density operator from its thermal equilibrium at time t of a spin ensemble of a protein with orientation of the molecule Ω specified by the 3 Euler angles (α, β, γ). $\hat{\hat{L}}(\Omega)$ is the Liouville commutator superoperater, which describes the unitary evolution of spins under the Hamiltonian that may depend on orientation Ω, and $\hat{\Gamma}$ is the stochastic diffusion operator which describes the random orientational motions of the nuclei of the spins in real space. The SLE deals with orientational space because all relevant stochastic NMR spin interactions considered here, which are the magnetic dipole-dipole (DD) coupling, the chemical shift anisotropy (CSA), and electric quadrupole coupling (QC), only depend on the orientational but not on overall translational effects.

For the mathematical representation, we choose the Wigner D-matrices $\mathcal{D}^{(l)}_{k,m}(\Omega)$ as the basis set of orientational space.[29] This basis set is convenient for expanding the Liouvillian,

since the isotropic and the anisotropic parts of the spin Hamiltonian can be expressed by the $l = 0$ term (Larmor precession, isotropic chemical shift and scalar J-couplings) and $l = 2$ terms (DD, CSA, QC), respectively. We capture the isotropic part by $\hat{\hat{H}}_{iso}$ and the anisotropic part by $\hat{\hat{Q}}_{k,m}$ so that the Liouvillian can be expressed as

$$\hat{\hat{L}}(\Omega) = \hat{\hat{H}}_{iso} + \sum_{k,m=-2}^{2} \mathcal{D}^{(2)}_{k,m}(\Omega)\hat{\hat{Q}}_{k,m} \tag{2}$$

We also expand the superoperators across an orthonormal spin basis $\hat{B}_\alpha$ by use of the trace metric:[32]

$$H_{iso,\alpha,\alpha'} = Tr(\hat{B}^\dagger_\alpha[\hat{H}_{iso}, \hat{B}_{\alpha'}]) \qquad Q_{k,m,\alpha,\alpha'} = Tr(\hat{B}^\dagger_\alpha[\hat{Q}_{k,m}, \hat{B}_{\alpha'}]) \tag{3}$$

We assume isotropic spherical tumbling in solution for both the free protein and the nanoparticle. The rotational diffusion operator $\hat{\Gamma}$ with rotational diffusion constant D then has eigenvalues and eigenfunctions[1,37]

$$\hat{\Gamma}\mathcal{D}^{(l)}_{k,m}(\Omega) = -Dl(l+1)\mathcal{D}^{(l)}_{k,m}(\Omega) \tag{4}$$

The assumption of isotropic spherical tumbling can be relaxed to accommodate anisotropic or non-spherical tumbling,[37] although at an increased computational cost.[38] When the density matrix is also expanded:

$$\hat{\rho}(\Omega, t) = \sum_{l=0}^{\infty} \sum_{k,m=-l}^{l} \sum_{\alpha} p^{(l)}_{k,m,\alpha}(t)\mathcal{D}^{(l)}_{k,m}(\Omega)\hat{B}_\alpha \tag{5}$$

where α extends over the entire spin basis $\hat{B}_\alpha$, we may use the Clebsch-Gordan coefficients $C^{J,M}_{j_1,m_1,j_2,m_2}$ and their orthogonality properties to yield the computationally solvable differential equation below, where it is implicitly assumed that invalid Clebsch-Gordan coefficients

are zero:

$$\partial_t p^{(l)}_{k,m,\alpha}(t) = \sum_{l'=max\{l-2,0\}}^{l+2} \sum_{k',m'=-l'}^{l'} \sum_{\alpha'} \Big(-\imath H_{iso,\alpha,\alpha'} \delta_{l,l'} \delta_{k,k'} \delta_{m,m'} \\ - \imath C^{l,k}_{2,k-k',l',k'} C^{l,m}_{2,m-m',l',m'} Q_{k-k',m-m',\alpha,\alpha'} - Dl(l+1) \delta_{\alpha,\alpha'} \delta_{l,l'} \delta_{k,k'} \delta_{m,m'} \Big) p^{(l')}_{k',m',\alpha'}(t) \quad (6)$$

Next, we include exchange between the protein in its free state and the nanoparticle-bound state. For this purpose, we double the orientation space by means of a direct sum with one half assigned as "P" and the other half as "NP". The diffusion operators between the two subspaces are then coupled with on-and off-rate constants, k_{on} and k_{off} (note that in practice k_{on} is a pseudo first-order rate constant derived from the second order rate constant k'_{on} via $k_{on} = [\mathrm{NP}] k'_{on}$). This yields two sets of coupled differential equations:

$$\partial_t p^{(l)}_{k,m,\alpha,P}(t) = \sum_{l',k',m',\alpha'} \Big(-\imath H_{iso,\alpha,\alpha'} \delta_{l,l'} \delta_{k,k'} \delta_{m,m'} - \imath C^{l,k}_{2,k-k',l',k'} C^{l,m}_{2,m-m',l',m'} Q_{k-k',m-m',\alpha,\alpha'} \\ - D_P l(l+1) \delta_{\alpha,\alpha'} \delta_{l,l'} \delta_{k,k'} \delta_{m,m'} \Big) p^{(l')}_{k',m',\alpha',P}(t) + k_{off} \hat{p}^{(l)}_{k,m,\alpha,NP}(t) - k_{on} \hat{p}^{(l)}_{k,m,\alpha,P}(t)$$

$$\partial_t p^{(l)}_{k,m,\alpha,NP}(t) = \sum_{l',k',m',\alpha'} \Big(-\imath H_{iso,\alpha,\alpha'} \delta_{l,l'} \delta_{k,k'} \delta_{m,m'} - \imath C^{l,k}_{2,k-k',l',k'} C^{l,m}_{2,m-m',l',m'} Q_{k-k',m-m',\alpha,\alpha'} \\ - D_{NP} l(l+1) \delta_{\alpha,\alpha'} \delta_{l,l'} \delta_{k,k'} \delta_{m,m'} \Big) p^{(l')}_{k',m',\alpha',NP}(t) + k_{on} \hat{p}^{(l)}_{k,m,\alpha,P}(t) - k_{off} \hat{p}^{(l)}_{k,m,\alpha,NP}(t) \quad (7)$$

This equation can be easily generalized by allowing for any number of states $\{s\}$ and allowing the Liouvillian to vary between these states. This generalized exchange model, given explicitly below, can then be used for the treatment of internal dynamics by a lattice jump

model and it allows the description of additional modes of exchange.

$$\partial_t p^{(l)}_{k,m,\alpha,s}(t) = \sum_{l',k',m',\alpha',s'} \Big(\big(-\imath H_{iso,s',\alpha,\alpha'} \delta_{l,l'} \delta_{k,k'} \delta_{m,m'} - \imath C^{l,k}_{2,k-k',l',k'} C^{l,m}_{2,m-m',l',m'} Q_{k-k',m-m',s',\alpha,\alpha'} \\ - D_{s'} l(l+1) \delta_{\alpha,\alpha'} \delta_{l,l'} \delta_{k,k'} \delta_{m,m'} \big) \delta_{s,s'} + (k_{s',s} - \sum_{s''} k_{s',s''} \delta_{s,s'}) \delta_{\alpha,\alpha'} \delta_{l,l'} \delta_{k,k'} \delta_{m,m'} \Big) p^{(l')}_{k',m',\alpha',s'}(t) \tag{8}$$

This set of coupled linear differential equations is computationally solvable as a matrix differential equation. When rewritten in this way, Eq. 7 becomes

$$\partial_t \mathbf{p}(t) = \mathbf{A}\mathbf{p}(t) \tag{9}$$

where

$$\mathbf{A} = -\imath \mathbf{L} \otimes \mathbf{I}_2 - \begin{bmatrix} \mathbf{D}_P & \mathbf{0} \\ \mathbf{0} & \mathbf{D}_{NP} \end{bmatrix} + \mathbf{I} \otimes \mathbf{K}$$

and $\mathbf{L}$ is the Liouvillian in matrix form, $\mathbf{D}_P$ and $\mathbf{D}_{NP}$ are the diffusion operator in matrix form, $\mathbf{I}_2$ is the 2×2 identity matrix, $\mathbf{I}$ is the identity matrix with the same size as $\mathbf{L}$, and $\mathbf{K}$ is the 2×2 exchange matrix describing binding kinetics between the two states. The resulting matrix $\mathbf{A}$ is quite large, non-Hermitian and not necessarily sparse unless the maximum l_{max} is very large. An arbitrary system with n_{state} states, n_{spin} spins, and with each spin having spin-I_j will have size $N_A \times N_A$ where

$$N_A = n_{state} \Big(\prod_{j=1}^{n_{spin}} (2I_j + 1)^2 \Big) \Big(\sum_{l=0}^{l_{max}} (2l+1)^2 \Big) \tag{10}$$

The second term in this equation is the spin-space contribution to the dimension of $\mathbf{A}$ and the third term denotes the contribution of orientational space to $\mathbf{A}$. For a 2-state, 2 spin-1/2 system with $l_{max} = 2$, as would be appropriate for simulating protein backbone ^{15}N relaxation, the matrix has size 1120×1120. Similarly, for a 2-state, spin-1 system, such as

deuterium ^2H with $l_{max} = 2$, the matrix has size 630×630.

The SLE as given in Eq. 9 is most conveniently solved by diagonalization of matrix $\mathbf{A}$:

$$\mathbf{A} = \mathbf{V}\mathbf{\Lambda}\mathbf{V}^{-1} \tag{11}$$

where diagonal matrix $\mathbf{\Lambda}$ contains the eigenvalues on its diagonal representing the resonance frequencies and relaxation rates of the corresponding spin dynamics eigenmodes, and the corresponding left and right eigenvectors represent the density matrices of those eigenmodes. As density matrix terms with $l > 0$ are experimentally not observable (since they represent non-equilibrium lattice states), these portions of the left and right eigenvectors can be ignored for relaxation analysis. Similarly, eigenpairs where the real part of the eigenvalue is very large represent modes of relaxation that will quickly decay to equilibrium and can be discarded. This leaves three much smaller matrices, one of which is diagonal, and allows the easy extraction of relaxation rates.

There are two principle methods by which we can extract a relaxation parameter $R(\hat{A} \rightarrow \hat{B})$, which is the rate of relaxation from starting density operator $\hat{A}$ to final density operator $\hat{B}$. Both involve expressing $\hat{A}$ and $\hat{B}$ as normalized vectors $\mathbf{a}$ and $\mathbf{b}$ in Liouville space as was done previously for the density operators $\hat{p}$. The most straightforward way is by simulating the NMR signal, as in Eq. 12. For many relaxation modes of practical interest, it is known from experiments that they decay in good approximation mono-exponentially. It is then possible to extract $R(\hat{A} \rightarrow \hat{B})$ by a numerical fit to the computed signal decay. Alternatively, it is possible to fit the instantaneous change in the signal $S(t)$ to determine the rate of relaxation.

$$S(t) = \mathbf{b}^\dagger \mathbf{V} e^{\mathbf{\Lambda} t} \mathbf{V}^{-1} \mathbf{a} \tag{12}$$

Relaxation rates can also be directly extracted from the eigenvalues given in $\mathbf{\Lambda}$. Each eigenvalue in this matrix represents a mode of relaxation where the corresponding right eigenvector

a is the starting spin state, and the corresponding left eigenvector **b** is the final spin state. For many commonly used relaxation parameters, such as the transverse relaxation of an $^{15}N-{}^{1}H$ system (without CSA) or a ^{2}H system undergoing quadrupolar relaxation, determination of the relaxation rate is trivial as the starting and observed density operators can be found in the eigenvectors and correspond to the same eigenvalue. However, for some cases this may not be as trivial. For example, a $^{15}N-{}^{1}H$ 2-spin 1/2 system with a ^{15}N CSA no longer has $\hat{N}_x$ (or $\hat{N}_y$, $\hat{N}_+$, etc.) as an eigenvector for determining R_2. Instead, the relevant eigenvectors correspond to the so-called TROSY line α and anti-TROSY line β,[39] each with its own eigenvalue. The transverse relaxation R_2, along with the cross-correlated cross-relaxation η_{xy}, can then be extracted from the sum and difference of the two eigenvalues, respectively.

Intramolecular protein motions can affect spin relaxation in major ways. In fact, their accurate characterization is often the main motivation to conduct NMR spin relaxation experiments at the first place.[40–42] Unlike the model-free analysis, which is the standard method for the analysis of relaxation data within the Redfield regime,[16] the representation of internal motions in the SLE is necessarily model-dependent. A computationally efficient way to account for these internal motions is an N-site lattice jump model that explicitly includes a discrete set of conformational substates that are in dynamic exchange with each other.[34–36] In this case, the model is formulated using Eq. 8 with N substates with the same $\hat{\hat{H}}_{iso}$ and $\hat{\Gamma}$ but different $\hat{\hat{Q}}_{k,m}$ in accordance with the relative orientations of the N substates.

RESULTS

It is instructive to analyze the behavior of differential $\Delta R_2(^{15}N)$ relaxation, depicted in Figure 1, in some more quantitative detail. The figure compares the numerical results of a set of SLE calculations with analytical BM and WCS results, whereby backbone $R_2(^{15}N)$ relaxation rates were calculated in the presence ($R_{2,ex}(^{15}N)$) and absence ($R_{2,P}(^{15}N)$) of

exchange with a slowly tumbling nanoparticle. The free protein, which is internally rigid, tumbles isotropically with rotational correlation time 4 ns. The protein-nanoparticle complex (bound state) tumbles isotropically as well but with a rotational correlation time of 1 μs due to its much larger size (e.g. 20 nm diameter). Relaxation occurs only through the magnetic dipole-dipole interaction to the amide hydrogen with a strength of 11.5 kHz, which corresponds to a $^{15}N - {}^{1}H$ bond length of 1.02 Å. Exchange occurs at a variable exchange rate and a bound population of 1% with identical chemical shifts in the free and bound state.

Several features are notable. At exchange rates below 3×10^1 s^{-1} and above 3×10^7 s^{-1}, $R_{2,ex}(^{15}N)$ approaches $R_{2,P}(^{15}N)$, i.e. $\Delta R_2(^{15}N) \rightarrow 0$, reflecting the insensitivity of R_2 to the presence of nanoparticles. In the slow k_{ex} regime, this is due to the exchange occurring slowly enough that the NMR signal decays bi-exponentially where the faster-decaying component has a 1% amplitude decaying with $R_{2,NP}(^{15}N)$, i.e. R_2 of a molecule that is fully bound to the nanoparticle, and a slower-decaying component with 99% amplitude that decays with $R_{2,P}(^{15}N)$. Because the fast decaying component has such a low amplitude and broad linewidth, after Fourier transformation the observed peak is only 1% lower in height than that of a protein in the absence of nanoparticles and for all practical purposes is thus indistinguishable from R_2 of a nanoparticle-free sample. In the very fast exchange regime, the effective rotational diffusion constant is the population-weighted average of D_P and D_{NP}, i.e. $D_{avg} = (1 - p_b)D_P + p_b D_{NP} \approx D_P$ leading to relaxation behavior that is dominated entirely by the free state. In the slow-to-intermediate exchange regime covering exchange rates from 3×10^1 s^{-1} to 3×10^3 s^{-1}, $\Delta R_2(^{15}N)$ significantly deviates from zero in line with BM and at variance with WCS. Conversely, at exchange rates in the intermediate-to-fast regime covering rates from 3×10^5 s^{-1} to 3×10^7 s^{-1}, $\Delta R_2(^{15}N)$ remains significantly different from zero, consistent with WCS and at variance with BM. In the exchange regime between these two regimes, i.e. the range from 3×10^3 s^{-1} to 3×10^5 s^{-1}, neither the BM nor WCS treatments are accurate as can be seen in Figure 1.

Similar types of behavior are observed for a variety of other situations as shown in

Figure 2. They include systems with different tumbling correlation times of the free and bound states, a near-static bound state, backbone ^{15}N relaxation through both magnetic dipole-dipole and CSA interactions, and quadrupolar relaxation of a ^{2}H spin. The exact range of the "intermediate regime" shifts depending on the overall interaction strength and tumbling correlation times. In all examples, the BM and WCS offer excellent approximations for the very slow and the very fast exchange regimes, but not vice versa, and both of these treatments are inadequate for the intermediate exchange regime. These types of simulations demonstrate the power of SLE to accurately cover the full range of exchange behavior and they allow one to assess the limits of the applicability regimes of the complementary BM and WCS treatments.

It is also notable that both BM (in the very fast limit) and WCS (in the very slow limit) converge to

$$\Delta R_2^* = p_b\big(R_{2,NP}{-}R_{2,P}\big) \tag{13}$$

where $R_{2,NP}$ and $R_{2,P}$ are obtained using Redfield theory. In this "intermediate exchange limit", ΔR_2^* of Eq. 13 has been observed consistently to be an upper limit for ΔR_2.

The effect of p_b and τ_{NP} on ΔR_2 is also of interest. As can be seen in Figure 3a, for small correlation times τ_{NP}, $\Delta R_2(^{15}N)$ scales linearly with τ_{NP}, then becoming asymptotic as the bound state approaches the situation of being bound to a static wall. This behavior holds most strongly for intermediate exchange rates and, as one would expect from the above discussion, the bound state size has little impact for slow or fast exchange as long as the bound state tumbles sufficiently more slowly than the free state. Figure 3b reveals that, for a minor bound population ($\leq 50\%$), the change in transverse relaxation ΔR_2 and longitudinal relaxation ΔR_1 scales linearly with the bound population, and these states can be normalized to be equal to the bound state population. The heteronuclear longitudinal relaxation ΔR_1 was found to be very weakly dependent on the exchange rate k_{ex} and bound state correlation time τ_{NP} (not shown), which makes $\Delta R_1(^{15}N)$ unsuitable to gain insights into these parameters.

Another useful observation is that transverse (and longitudinal) relaxation in the exchanging system were found to be monoexponential to high accuracy for all parameter sets tested here. For illustration, several spectra have been generated in Figure 4a, in which all simulated spectra are Lorentzian to high accuracy even when the bound population is sizeable. Spectra predicted by SLE are shown in Figure 4b for gradually increasing populations when binding to a near-static wall ($\tau_{NP} = 1\ ms$). They demonstrate that the peak shape is in good approximation Lorentzian up to 40% bound (i.e. the time-domain signal decays monoexponentially), whereas at about 60% bound, the peak is clearly no longer Lorentzian, and starting at 80% bound a solid-state type Pake pattern begins to emerge as expected.

Among the most useful biophysical information about proteins that can be gained from NMR relaxation experiments is the amount of internal dynamics at individual protein sites in the form of a site-specific Lipari-Szabo order parameter S^2 and an internal correlation time τ_{int}.[16] S^2 is a measure of the motional restriction of the reorientation of a dipolar vector, such as a $^{15}N - ^{1}H$ bond, whereby a low S^2 generally reflects large amplitude motions and vice versa. Within the SLE framework, we model internal motion stochastically as a 2-site lattice jump that occurs independently of rotational diffusion and nanoparticle binding. The resulting $\Delta R_2(^{15}N)$ shown in Figure 5 are normalized with respect to $\Delta R_2(^{15}N)$ of an internally rigid system, $\Delta R_{2,norm} = \Delta R_2(^{15}N)/\Delta R_{2,rigid}(^{15}N)$. This means that a system with $S^2 = 1$ will appear as a horizontal line with $\Delta R_{2,norm} = 1$, whereas the presence of internal motion ($S^2 < 1$) will differentially scale $\Delta R_{2,norm}$ depending on k_{ex} and τ_{int}, whereby τ_P and τ_{NP} were kept fixed at their standard values of 4 ns and 1 μs. The normalized ratio $S^2_{app} = \Delta R_{2,norm}$ is plotted along the y-axes of Figure 5. The figure depicts the interplay between $\Delta R_{2,norm}$ (S^2_{app}) and S^2, k_{ex}, and τ_{int}.

Several features in Figure 5 are notable. First, except for the numerical range of the y-axes, corresponding curves of the same color across the panels are remarkably similar to each other, which means that the actual order parameter S^2 leads to an overall scaling independent of τ_{int}. This behavior is analogous to a free protein for which $S^2 = R_{2,P}/R_{2,P,rigid}$ when τ_{int}

is much faster than τ_P. In each panel, the curves can be partitioned into three distinct k_{ex} regimes that show characteristic behavior in terms of the apparent S^2 properties. For very slow exchange rates (limit to left), S^2_{app} approaches 1 independent of τ_{int}, which is a consequence of $\Delta R_2 = 0$ for very slow exchange as discussed above. For very fast exchange (limit to right), it can be shown that $\Delta R_2 \propto R_{2,P}$ and, hence, S^2_{app} overestimates the true S^2 when τ_{int} is near or larger than τ_P, which is akin to standard model-free analysis of spin relaxation data of the free protein. However, neither of these conditions is particularly relevant in practice as they both lead to very small ΔR_2's (provided that the difference between τ_{NP} and τ_P is large) and, hence, are challenging to measure accurately.

Most interesting in practice is the behavior for intermediate exchange rates where ΔR_2 is of significant size. In this case, the intermediate exchange limit of Eq. 13 roughly applies, which means $\Delta R_2 \propto R_{2,NP}$. In this regime S^2_{app} changes most significantly when $\tau_{int} \approx \tau_{NP}$ as can be seen between the cyan and yellow lines. Therefore, in the intermediate exchange regime, covering a broad range of k_{ex} values, through S^2_{app} one can monitor internal dynamics taking place on timescales τ_{int} far slower than accessible by traditional spin relaxation experiments of free protein, which only extends from ps to ns (i.e. faster than τ_P). As a direct consequence, depending on the nanoparticle size, dynamics processes can be observed with τ_{int} as long as μs or even beyond. This property of nanoparticle-assisted spin relaxation has been exploited recently to study the presence or absence of internal protein dynamics on the previously unchartered protein dynamics timescales from tens of ns to low μs.[14,15] The k_{ex} thresholds that separate the different regimes follow consistent rules. The transition from the slow to the intermediate regime occurs at a k_{ex} range around the difference $R_{2,NP} - R_{2,P}$. In contrast, the intermediate regime changes to fast around $k_{ex} \approx 1/\tau_{int}$. Taken together, these conditions imply that S^2_{app} is a good approximation for S^2 as long as $R_{2,NP} - R_{2,P} < k_{ex} < 1/\tau_{int}$.

DISCUSSION AND CONCLUSION

The SLE provides a mathematically and physically rigorous framework for the accurate computation of dissipative protein spin dynamics behavior under protein-nanoparticle interactions on all practically relevant timescales of overall tumbling, exchange, and internal motions and bound populations. The SLE is able to accurately reproduce the results from existing approximate treatments of BM and WCS in the limits of the slow and fast exchange, respectively. Furthermore, the SLE is able to quantitatively describe the applicability range of these approximate treatments as shown in Figure 1. BM is valid as long as k_{ex} is much slower than the stochastically modulated anisotropic spin interactions that give rise to spin relaxation, while WCS is valid if k_{ex} is much faster. Furthermore, the location of the maximum of the ΔR_2 vs. k_{ex} curve, and thus the exchange rate where relaxation deviates most from either theory, is proportional to the anisotropic spin interaction strength. Notably, this is also the region where nanoparticles have the greatest effect on transverse spin relaxation, and experimental data will be most sensitive to biophysical parameters of interest. For the system of Figure 1, this regime encompasses exchange rates from $10^3\ s^{-1}$ to $10^6\ s^{-1}$, which for $p_b = 1\%$ corresponds to $k_{on} \approx 10^1 - 10^4\ s^{-1}$ and $k_{off} \approx 10^3 - 10^6\ s^{-1}$. For a typical nanoparticle concentration of 1 μM, the optimal range of second-order binding rate constants is then $k'_{on} \approx 10^7 - 10^{10}\ s^{-1}M^{-1}$.

A practical concern for the numerical implementation of the SLE is the size of the non-Hermitian matrix that must be diagonalized. Eq. 10 shows the steep scaling of the matrix size and associated computational costs, especially for larger spin systems or systems requiring large l_{max}, as is the case in the vicinity of the static limit. Fortunately, there are several ways to mitigate this problem. First, if the spin system geometry is axially symmetric (e.g. a single dipolar interaction or an axially symmetric CSA tensor), the spherical harmonics may be used instead of the Wigner matrices for the expansion of orientational space. If the secular approximation is taken for all terms in the Hamiltonian, the number of accessible spin terms may be significantly reduced depending on the relaxation pathway of interest. If taken

in concert with axial symmetry of the spin system, then the $k \neq 0$ terms in the orientation space also become trivial. These allow for high l_{max} at affordable computational cost such as those needed for Figure 4b. Fortunately, for all systems ran for the examples shown in the other figures, it was found that $l_{max} = 2$ is sufficient. This reduced the time needed for the simulation of the SLE results shown in Figure 1 to 540 ms when run in Python 2.7 with the NumPy library[43] on a desktop computer using an Intel i7-7700 CPU and allowing NumPy to utilize all 4 cores. In turn, the longest calculation, which is the one of the exchanging system with internal dynamics of Figure 5, took 17 s. Indeed, for systems with anisotropic Hamiltonian strength on the order of the N-H dipole-dipole coupling (11.5 kHz), it turned out that $l_{max} > 2$ was only required for systems with $\tau_{NP} > 100\ \mu s$ and $p_b > 0.4$.

Because both ΔR_2 and ΔR_1 are monotonic with respect to τ_{NP} and linear with p_b (see Figure 3), their interpretation from experiment is relatively straightforward. However, the more complex and non-monotonic dependence of ΔR_2 on k_{ex} implies that the quantitative extraction of k_{ex} may be ambiguous when only a single relaxation parameter, such as $R_2(^{15}N)$, is available. Representative simulations demonstrate the quantitative dependence of ΔR_2 on both thermodynamic and kinetic parameters, including bound vs. free populations, exchange rate constant, rotational tumbling correlation time of the bound and free states, and internal dynamics amplitude and timescale. Due to the increase of the number of model parameters compared to relaxation studies of free protein, the interpretation of experimental ΔR_2 data can benefit from information from complementary sources, such as the nanoparticle size, e.g. from dynamic light scattering (DLS), analytical centrifugation (AUC), or transmission electronmicroscopy (TEM), from which τ_{NP} can be obtained with reasonable accuracy based on the Debye-Stokes-Einstein relationship and τ_P from NMR experiments of free protein. This still leaves several model parameters to be determined, which can be achieved by ΔR_2 measurements of other spins experiencing spin interactions of different strengths by utilizing that they will distinctly respond to k_{ex}. For biomolecules, these may include relaxation processes involving ^{15}N, ^{13}C, and ^{2}H spins.

In this work, we assumed that nanoparticles are in good approximation monodispersed. In practice, polydispersity of nanoparticles can be experimentally assessed by dynamic light scattering or transmission electron microscopy. When necessary, a discrete size distribution of nanoparticles can be modeled by extending the SLE to include separate nanoparticle species with different tumbling correlation times, which however will concomitantly increase the SLE dimension and associated computational cost.

Besides obtaining quantitative information about bound population and k_{ex}, which are global parameters, ΔR_2 measurements offer information about internal dynamics. They provide an unobscured view of internal motions for many atomic sites in a protein, both on the backbone and the side-chains, taking place on a vast range of internal timescales from ps to sub-μs, μs or even beyond that in the past have been very hard to access by NMR or any other experimental method. At least some of these motions are expected to be biologically important.[14] From an experimental perspective, the read-out of S^2 values is rather straightforward as it only requires the measurement of transverse spin relaxation rates, once in the absence and once in the presence of nanoparticles in the intermediate exchange regime, followed by global normalization of their difference. We have focused here on transverse spin relaxation behavior, but the SLE is equally well applicable to other relaxation processes, including homonuclear longitudinal relaxation and cross-correlated relaxation as well as (semi-)selective saturation experiments, such as CEST and DEST, which have their own specific dependencies on model parameters and, hence, can be useful for the complementary experimental characterization of these parameters.

AUTHOR INFORMATION

Corresponding Author

*E-mail: bruschweiler.1@osu.edu

Notes

The authors declare no competing financial interest.

ACKNOWLEDGEMENTS

We thank Xinyao Xiang for discussion. This work was supported by the NSF (award MCB-1715505) and the National Institutes of Health (grant R01GM06604).

References

(1) Favro, L. D. Theory of the Rotational Brownian Motion of a Free Rigid Body. *Phys. Rev.* **1960**, *119*, 53–62.

(2) Ni, F. Recent developments in transferred NOE methods. *Prog. Nucl. Mag. Res. Sp.* **1994**, *26*, 517 – 606.

(3) Post, C. B. Exchange-transferred NOE spectroscopy and bound ligand structure determination. *Curr. Opin. Struc. Biol.* **2003**, *13*, 581—588.

(4) Halle, B.; Denisov, V. Magnetic relaxation dispersion studies of biomolecular solutions. *Method. Enzymol.* **2001**, *338*, 178—201.

(5) Bertini, I.; Fragai, M.; Luchinat, C.; Talluri, E. Water-Based Ligand Screening for Paramagnetic Metalloproteins. *Angew. Chem., Int. Ed.* **2008**, *47*, 4533–4537.

(6) Mayer, M.; Meyer, B. Characterization of Ligand Binding by Saturation Transfer Difference NMR Spectroscopy. *Angew. Chem., Int. Ed.* **1999**, *38*, 1784–1788.

(7) Angulo, J.; Nieto, P. M. STD-NMR: application to transient interactions between biomolecules-a quantitative approach. *Eur. Biophys. J.* **2011**, *40*, 1357—1369.

(8) van Zijl, P. C. M.; Yadav, N. N. Chemical exchange saturation transfer (CEST): What is in a name and what isn't? *Magn. Reson. Med.* **2011**, *65*, 927–948.

(9) Vallurupalli, P.; Bouvignies, G.; Kay, L. E. Studying "Invisible" Excited Protein States in Slow Exchange with a Major State Conformation. *J. Am. Chem. Soc.* **2012**, *134*, 8148–8161.

(10) Clore, G. M.; Tang, C.; Iwahara, J. Elucidating transient macromolecular interactions using paramagnetic relaxation enhancement. *Curr. Opin. Struc. Biol.* **2007**, *17*, 603 – 616.

(11) Clore, G. M.; Iwahara, J. Theory, Practice, and Applications of Paramagnetic Relaxation Enhancement for the Characterization of Transient Low-Population States of Biological Macromolecules and Their Complexes. *Chem. Rev.* **2009**, *109*, 4108–4139.

(12) Fawzi, N. L.; Ying, J.; Ghirlando, R.; Torchia, D. A.; Clore, G. M. Atomic-resolution dynamics on the surface of amyloid-β protofibrils probed by solution NMR. *Nature* **2011**, *480*, 268–272.

(13) Anthis, N. J.; Clore, G. M. Visualizing transient dark states by NMR spectroscopy. *Q. Rev. Biophys.* **2015**, *48*, 35–116.

(14) Xie, M.; Yu, L.; Bruschweiler-Li, L.; Xiang, X.; Hansen, A. L.; Brüschweiler, R. Functional protein dynamics on uncharted time scales detected by nanoparticle-assisted NMR spin relaxation. *Sci. Adv.* **2019**, *5*.

(15) Wardenfelt, S.; Xiang, X.; Xie, M.; Yu, L.; Bruschweiler-Li, L.; Brüschweiler, R. Broadband Dynamics of Ubiquitin by Anionic and Cationic Nanoparticle Assisted NMR Spin Relaxation. *Angew. Chem., Int. Ed.* **2021**, *60*, 148–152.

(16) Lipari, G.; Szabo, A. Model-free approach to the interpretation of nuclear magnetic resonance relaxation in macromolecules. 1. Theory and range of validity. *J. Am. Chem. Soc.* **1982**, *104*, 4546–4559.

(17) McConnell, H. M. Reaction Rates by Nuclear Magnetic Resonance. *J. Chem. Phys.* **1958**, *28*, 430–431.

(18) Vallurupalli, P.; Sekhar, A.; Yuwen, T.; Kay, L. E. Probing conformational dynamics in biomolecules via chemical exchange saturation transfer: a primer. *J. Biomol. NMR* **2017**, *67*, 243—271.

(19) Wong, V.; Case, D. A.; Szabo, A. Influence of the coupling of interdomain and overall motions on NMR relaxation. *P. Natl. Acad. Sci. USA* **2009**, *106*, 11016–11021.

(20) Kubo, R. Stochastic Liouville Equations. *J. Math. Phys.* **1963**, *4*, 174–183.

(21) Kubo, R. *Advances in Chemical Physics*; John Wiley & Sons, Ltd, 1969; pp 101–127.

(22) Moro, G.; Freed, J. H. Efficient computation of magnetic resonance spectra and related correlation functions from stochastic Liouville equations. *J. Phys. Chem.* **1980**, *84*, 2837–2840.

(23) Peng, Z.; Ho, C. An exact evaluation of nuclear spin-lattice relaxation for a two-site jump model. *J. Magn. Reson.* **1989**, *82*, 318 – 336.

(24) Halle, B. Spin dynamics of exchanging quadrupolar nuclei in locally anisotropic systems. *Prog. Nucl. Mag. Res. Sp.* **1996**, *28*, 137–160.

(25) Brüschweiler, R. Nuclear spin relaxation and non-ergodic quasi-equilibria. *Chem. Phys. Lett.* **1997**, *270*, 217 – 221.

(26) Nevzorov, A. A.; Freed, J. H. Spin relaxation by dipolar coupling: From motional narrowing to the rigid limit. *J. Chem. Phys.* **2000**, *112*, 1413–1424.

(27) Abergel, D.; Palmer III, A. G. On the use of the stochastic Liouville equation in nuclear magnetic resonance: Application to R1 relaxation in the presence of exchange. *Concept. Magn. Reson. A* **2003**, *19A*, 134–148.

(28) Trott, O.; Abergel, D.; Palmer III, A. G. An average-magnetization analysis of R 1 relaxation outside of the fast exchange limit. *Mol. Phys.* **2003**, *101*, 753–763.

(29) Edwards, L. J.; Savostyanov, D.; Nevzorov, A.; Concistrè, M.; Pileio, G.; Kuprov, I. Grid-free powder averages: On the applications of the Fokker–Planck equation to solid state NMR. *J. Magn. Reson.* **2013**, *235*, 121 – 129.

(30) Kuprov, I. Fokker-Planck formalism in magnetic resonance simulations. *J. Magn. Reson.* **2016**, *270*, 124 – 135.

(31) Pell, A. J.; Pintacuda, G.; Grey, C. P. Paramagnetic NMR in solution and the solid state. *Prog. Nucl. Mag. Res. Sp.* **2019**, *111*, 1 – 271.

(32) Ernst, R. R.; Bodenhausen, G.; Wokaun, A., et al. *Principles of nuclear magnetic resonance in one and two dimensions*; Clarendon Press Oxford, 1987; Vol. 14.

(33) Schneider, D. J.; Freed, J. H. *Advances in Chemical Physics*; John Wiley Sons, Ltd, 1989; Chapter 10, pp 387–527.

(34) Wallach, D. Effect of Internal Rotation on Angular Correlation Functions. *J. Chem. Phys.* **1967**, *47*, 5258–5268.

(35) London, R. E.; Avitabile, J. Calculation of carbon-13 relaxation times and nuclear Overhauser enhancements in a hydrocarbon chain undergoing gauche-trans isomerism. *J. Am. Chem. Soc.* **1977**, *99*, 7765–7776.

(36) Wittebort, R. J.; Szabo, A. Theory of NMR relaxation in macromolecules: Restricted diffusion and jump models for multiple internal rotations in amino acid side chains. *J. Chem. Phys.* **1978**, *69*, 1722–1736.

(37) Berne, B. J.; Pecora, R. *Dynamic Light Scattering: With Applications to Chemistry, Biology, and Physics*; Dover Publications, 2000.

(38) Lehner, J.; Stoll, S. Modeling of motional EPR spectra using hindered Brownian rotational diffusion and the stochastic Liouville equation. *J. Chem. Phys.* **2020**, *152*, 094103.

(39) Zuiderweg, E. R.; Rousaki, A. Gradient-enhanced TROSY described with Cartesian product operators. *Concept. Magn. Reson. A* **2011**, *38A*, 280–288.

(40) Woessner, D. E. Nuclear Magnetic Dipole—Dipole Relaxation in Molecules with Internal Motion. *J. Chem. Phys.* **1965**, *42*, 1855–1859.

(41) Cavanagh, J.; Fairbrother, W. J.; Palmer III, A. G.; Skelton, N. J. *Protein NMR spectroscopy: principles and practice*; Elsevier, 1995.

(42) Korzhnev, D.; Billeter, M.; Arseniev, A.; Orekhov, V. NMR studies of Brownian tumbling and internal motions in proteins. *Prog. Nucl. Mag. Res. Sp.* **2001**, *38*, 197 – 266.

(43) Harris, C. R.; Millman, K. J.; van der Walt, S. J.; Gommers, R.; Virtanen, P.; Cournapeau, D.; Wieser, E.; Taylor, J.; Berg, S.; Smith, N. J.; Kern, R.; Picus, M.; Hoyer, S.; van Kerkwijk, M. H.; Brett, M.; Haldane, A.; del Río, J. F.; Wiebe, M.; Peterson, P.; G'erard-Marchant, P.; Sheppard, K.; Reddy, T.; Weckesser, W.; Abbasi, H.; Gohlke, C.; Oliphant, T. E. Array programming with NumPy. *Nature* **2020**, *585*, 357–362.

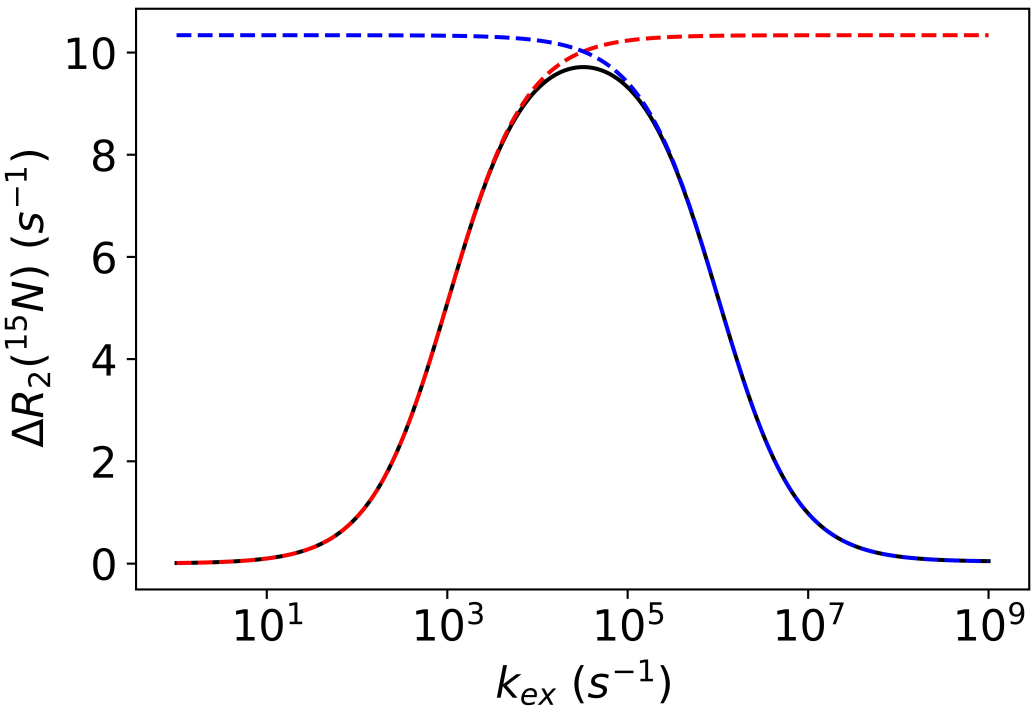

Figure 1: Change in backbone $R_2(^{15}N)$ relaxation between a small protein with τ_P of 4 ns tumbling correlation time undergoing exchange between its free form and a nanoparticle-bound state with a tumbling correlation time τ_{NP} of 1 μs as a function of the exchange rate k_{ex} with a constant bound population p_b of 1%. Relaxation occurs exclusively through the magnetic dipolar interaction with a directly bonded ^1H spin with a coupling constant of 11.5 kHz. Relaxation profiles were computed by BM (red dashed line), WCS (blue dashed line), and SLE (black line).

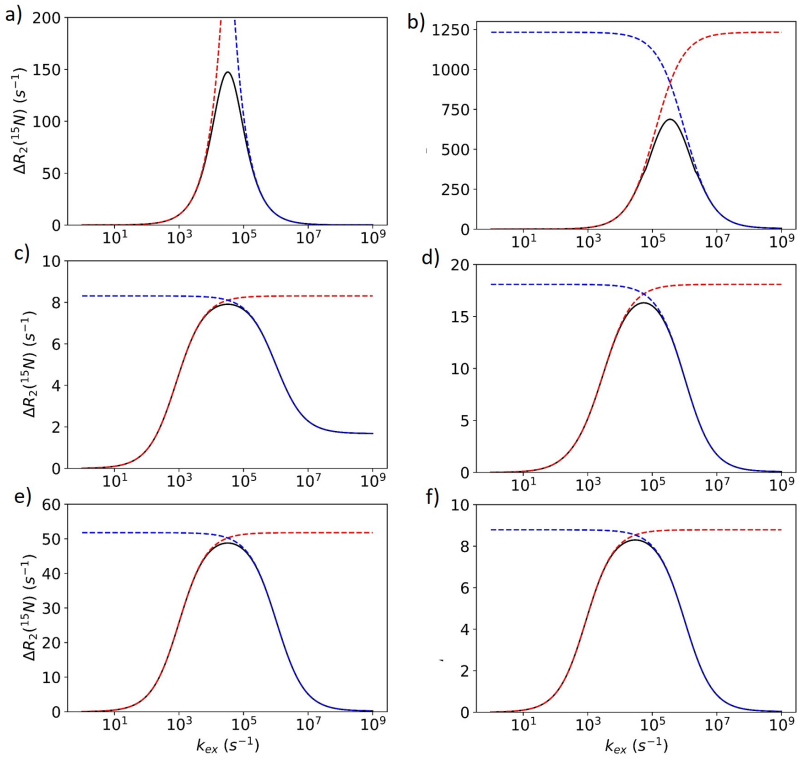

Figure 2: Change in backbone R_2 spin relaxation rate between a free protein and a protein exchanging with a nanoparticle or static wall at 850 MHz ^1H proton resonance frequency. The system is the same as in Figure 1 except that (a) the protein is exchanging with a bound-to-wall state, (b) the spin being observed is ^2H undergoing quadrupolar relaxation with a quadrupolar coupling constant of 167 kHz, (c) the free state has a rotational correlation time of 200 ns, (d) the ^{15}N spin experiences in addition to the magnetic dipole-dipole interaction also a CSA of -173 ppm, (e) the bound population is increased to 5%, and (f) the N-H bond vector is undergoing very fast internal reorientational 2-site lattice jump motion with an order parameter S^2 of 0.85. Panel (c) does not follow the common trend of $\Delta R_2(^{15}N) \rightarrow 0$ for fast k_{ex} because $D_{avg} \approx D_P$ no longer holds. Relaxation values were determined by BM (red dashed), WCS (blue dashed), and SLE (black lines) treatments.

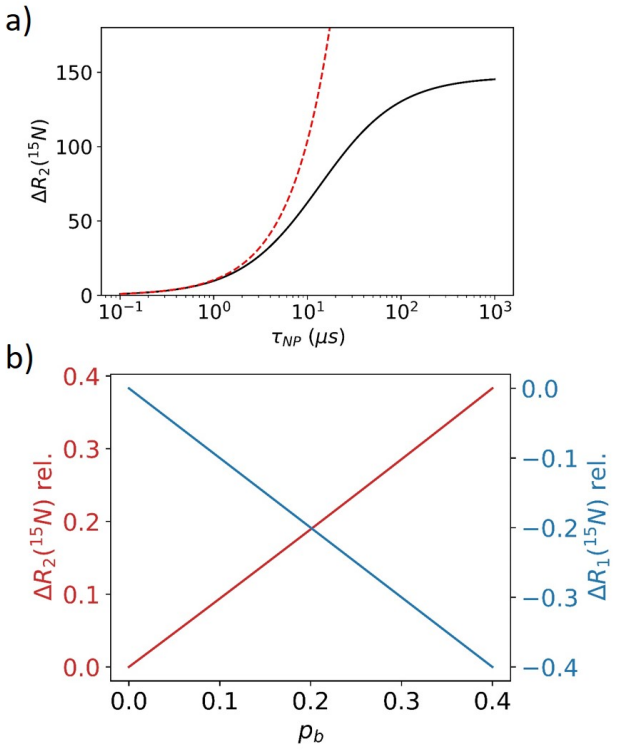

Figure 3: Change in backbone $R_2(^{15}N)$ spin relaxation rate between a free protein and a protein exchanging with a nanoparticle. (a) System is as described for Figure 1 except that bound state correlation time τ_{NP} is varied whereby the exchange rate is kept constant at $3 \times 10^4\ s^{-1}$. Relaxation rates were computed by SLE (black). Also indicated is the predicted relaxation value if scaled linearly with bound state rotational correlation time τ_{NP} according to Redfield relaxation theory (red dashed line). (b) System is as described for Figure 1 except that the bound state population is varied (with constant exchange rate $3 \times 10^4\ s^{-1}$). Relaxation values for R_2 (red) and R_1 (blue) were determined by SLE.

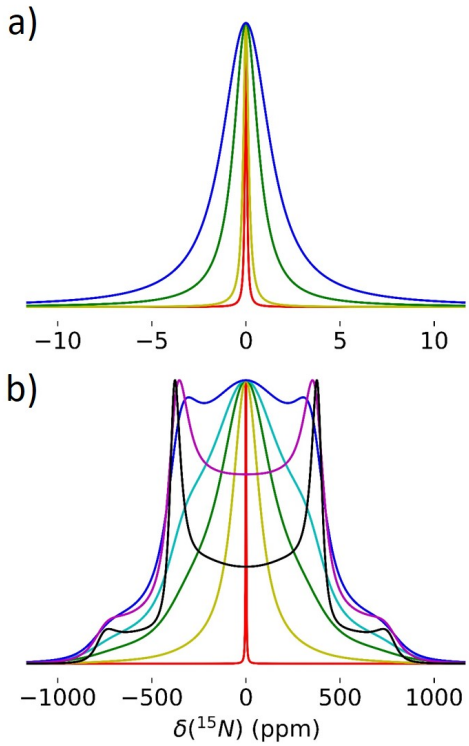

Figure 4: Peak shapes for a backbone ^{15}N resonance as described for Figure 1. (a) The exchange rate k_{ex} was fixed at 3×10^4 s^{-1} and the bound population was set to 1%. The bound state correlation time was 0.1 μs (red), 1 μs (yellow), 10 μs (green), and 100 μs (blue). (b) The exchange rate k_{ex} was fixed at 3×10^4 s^{-1} and the bound state correlation time τ_{NP} was set to 1 ms corresponding to a near static wall condition. The bound population was 1% (red), 40% (yellow), 60% (green), 70% (cyan), 80% (blue), 90% (magenta), and 100% (black).

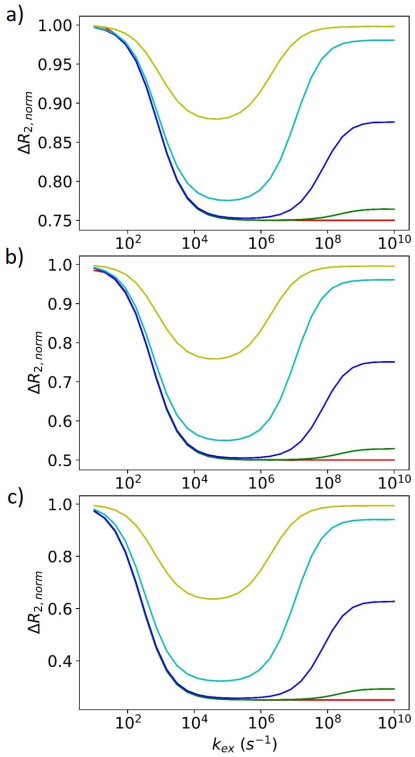

Figure 5: Change in backbone $R_2(^{15}N)$ relaxation by the presence of internal dynamics as a fraction of change, S^2_{app}, in backbone R_2 relative to an internally static system. The system is otherwise as described for Figure 1 with a binding exchange rate of 3×10^4 s^{-1}. Internal dynamics are modeled using a 2-site lattice jump with order parameter 0.75 (a), 0.5 (b), and 0.25 (c) and internal correlation time 1 μs (yellow), 100 ns (cyan), 10 ns (blue), 1 ns (green), and 1 ps (red).

Graphical TOC Entry